Gil-Santos, A.; Moelans, N.; Hort, N.; Van der Biest, O.:

Identification and description of intermetallic compounds in Mg–Si–Sr cast and heat-treated alloys

In: Journal of Alloys and Compounds (2016) Elsevier

DOI: 10.1016/j.jallcom.2016.01.221

Identification and description of intermetallic compounds in Mg-Si-Sr cast and heat-treated alloys

A Gil-Santos[1*], N Moelans[1], N Hort[2], O Van der Biest[1]

[1]*Department of Materials Engineering, KU Leuven, Kasteelpark Arenberg, 44, 3001 Leuven, Belgium*
[2]*Magnesium Innovation Centre (MagIC), Helmholtz-Zentrum Geesthacht, Max-Planck-Strasse 1, 21502 Geesthacht, Germany*

Corresponding author e-mail: andrea.gilsantos@mtm.kuleuven.be
*Present address: andrea.gil.santos@hotmail.com

Abstract

The ternary Mg-Si-Sr system is experimentally investigated in this work. Twelve compositions located in the Mg rich corner of the ternary system are processed. The microstructure and phase content of the different alloys are analysed in the as-cast condition and after additional heat treatments.

Apart from the Mg matrix, various intermetallic phases are observed. The binary compounds Mg_2Si and $Mg_{17}Sr_2$ are identified, as well as, two ternary phases MgSiSr and $MgSi_2Sr$.The morphology and distribution of the intermetallic phases is discussed with particular interest on the ternary intermetallics MgSiSr and $MgSi_2Sr$ for which only scarce information is available in literature. The phase stability and the stability of the intermetallic phases in these alloys are discussed.

The Mg rich side of the Mg-Si-Sr phase diagram is constructed based on descriptions of the binary phase diagrams Mg-Si, Mg-Ca and Ca-Si from literature and assuming complete solubility (i.e. a line compound) between the ternary phase MgSiSr and the binary phase Sr_2Si. It is also assumed that $MgSi_2Sr$ is a stoichiometric compound. These assumptions were made based on the chemical similarities between Ca and Sr and between Si and Sn, and the similarity in crystal structures between the two studied ternary compounds of the Mg-Si-Sr diagram and the ternary compounds present in the Ca-Mg-Si and Mg-Sn-Sr system. A good agreement is found between the constructed phase diagram and the experimental results.

Keywords: intermetallics; metals and alloys; microstructure; phase diagrams; scanning electron microscopy, SEM; thermodynamic modelling.

1. Introduction

The potential application of Mg rich alloys as resorbable materials for biomedical devices has been widely discussed in the last decade [1-4]. With the general objective of finding a new alloy system with low toxicity, the alloy elements Si and Sr have been selected as promising candidates.

The utility of a potential system depends on aspects as the mechanical properties, degradation behaviour or castability. Some of these properties are usually determined by the metallographic structure which is the consequence of the solidification conditions and sample composition. Microstructural information can be predicted using thermodynamic databases with the help of commercial softwares such as Pandat [5], Thermo-Calc [6] or Factsage [7]. The reliability of this type of calculations is based on the consistency of the employed database. The quality of the databases depends on the amount of available information on the phase diagrams and thermodynamic properties of the phases. The more trustable information is available about the system the more accurate the thermodynamic description will be.

In particular, the published information on the Mg-Si-Sr ternary system is scarce and it does not include any thermodynamic data. The available information collected from literature refers to the existence of some ternary compounds, related sometimes with its antiferroelectric behavior [8]. Five different compounds have been synthesized within the Mg-Si-Sr system, they are: MgSiSr [9], $MgSiSr_2$, $Mg_2Si_{10}Sr_{11}$ [10], $Mg_2Si_{20}Sr_{13}$ [11] and $Mg_{16.6}Si_{13}Sr_{6.3}$ [12]. However, only the crystal structure of these ternary compounds is known. Further information on the ternary Mg-Sr-Si system is absent. In this work, the phase equilibria of the two ternary phases MgSiSr and $MgSi_2Sr$ located in the Mg rich corner region are experimentally identified.

The aim of this study is to deepen the knowledge on the Mg rich corner of the Mg-Sr-Si system by performing a set of solidification experiments and subsequent heat treatments. A methodology to investigate the evolution of the microstructure together with the precipitation sequence of intermetallic phases is presented. Then a thermodynamic description of the 2 ternary phases MgSiSr and $MgSi_2Sr$ is proposed and used to generate a ternary database describing the Mg-rich side of the Mg-Si-Sr system. The calculated phase equilibria obtained with this database are compared with the experimental.

2. Theoretical calculations

In the works of Eisenman et al. and Currao et al. [9, 10], it is found that the ternary compounds MgSiSr and $MgSi_2Sr$ have both a orthorombic crystal systems with Pnma-62 space group. Considering the chemical similarities between Ca and Sr and between Si and Sn, we can assume that the Mg-Si-Sr phase diagram has similarities with the Mg-Si-Ca and Mg-Sn-Sr phase diagram. Especially since the structure of the ternary MgSiSr phase is similar to the crystal structure of the MgSiCa compound reported in the Mg-Si-Ca system [13] and that of the MgSnSr compound reported in the Mg-Sn-Sr system [14].

Since the MgSiSr and the Sr_2Si phase have the same crystal structure, it is assumed in this work that there is complete solubility between both compounds (i.e. they form a line compound). This assumption was also based on the observation that MgCaSi and $SiCa_2$ exhibit the same crystal structure and show full solubility in the Mg-Ca-Si and the same for MgSrSn and $SnSr_2$ in the Mg-Sr-

Sn system. For the other ternary compound, $MgSi_2Sr$, a stoichiometric description was selected similar to that used for $MgSi_2Ca$ in reference [13].

The thermodynamic parameters chosen for the two ternary phases are given in Table 1.

With these descriptions for the ternary phases and using the most recently published thermodynamic descriptions of the three binaries Mg-Si, Mg-Sr and Si-Sr, a thermodynamic database for Mg-Si-Sr was composed and the Mg-rich side of the ternary diagram at 300°C was calculated (figure 1). The binary descriptions with their thermodynamic parameters and models used in this work are taken from the assessments published by respectively, Schick et al., Zhong et al. and Garay et al. [15-17]. The Gibbs energies of pure Mg, Si and Sr are taken from the Scientific Group Thermodata Europe (SGTE) pure element database [18]. The software Thermo-Calc 2015b was used to generate the database and for the phase diagram calculation .

Table 1. Thermodynamic parameters used in this work, together with the descriptions of the binaries of Schick et al., Zhong et al. and Garay et al. [15-17], to describe the Mg-rich side of the Mg-Si-Sr ternary system

Phase	Parameters	Reference
Sr_2Si (Mg,Sr)(Si)(Sr)	$G^{0,\,Sr_2Si}_{Mg,Sr:Si:Sr} = 2G^{0,fcc}_{Sr} + G^{0,diamond}_{Si} - 122329.65 + 5.48\,T$	[17]
MgSiSr (Mg,Sr)(Si)(Sr)	$G^{0,MgSrSi}_{Mg,Sr:Si:Sr} = G^{0,hcp}_{Mg} + G^{0,fcc}_{Sr} + G^{0,diamond}_{Si} - 180000 + 50\,T$	This work
$MgSi_2Sr$ (Mg)$(Si)_2$(Sr)	$G^{0,MgSi_2Sr}_{Mg:Sr:Si} = G^{0,hcp}_{Mg} + G^{0,fcc}_{Sr} + 2G^{0,diamond}_{Si} - 233827$	This work

In order to make the analysis easier the intermetallic names were shortened to a few characters, as listed in table 2:

Table 2. Correspondence between intermetallic compound names and their identification used in this work

Intermetallic compound	Name
$Mg_{17}Sr_2$	M17
Mg_2Si	M2
MgSiSr	M111
$MgSi_2Sr$	M121

From the calculated isothermal section at 300°C (figure 1) three regions are expected with different phase constitution and they are defined by the At%Si:At%Sr ratio. A combination of Mg, M17 and M121 is expected for the Sr rich alloys (At%Si:At%Sr <1). For the case of the Si rich alloys (At%Si:At%Sr >2), Mg, M2 and M111 are predicted. For the alloys with a At%Si:At%Sr ratio closer to 1,5 (1< At%Si:At%Sr <2), the expected phases are the two ternary compounds M111 and M121 together with the Mg matrix

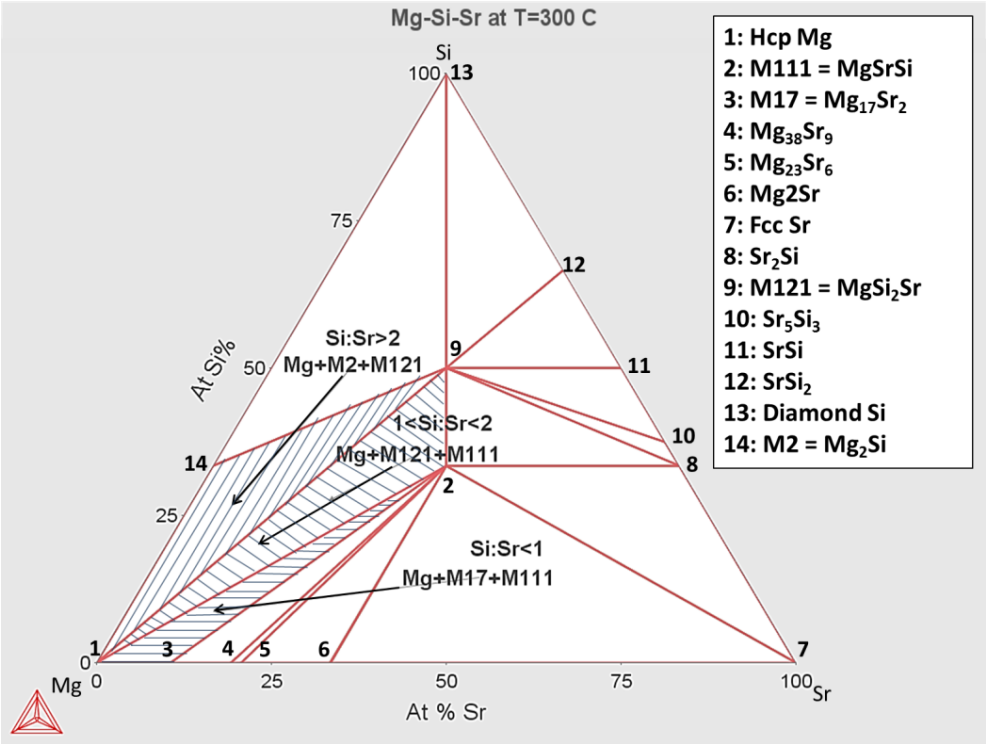

Figure 1. Calculated isothermal section at 300°C from the Mg-Si-Sr system including the identification of the regions in the Mg rich corner, using the database developed in this work.

3. Materials and methods

The Mg-Si-Sr alloys were processed by permanent mould gravity casting at Magnesium Innovation Centre MagIC (Geesthacht, Germany). Cylinders of 1.8 cm diameter and 20 cm length were cast. Raw materials consisted of Mg ingots (99.9 %), Si granulates (99.9 %) and Sr chips (97.3 %). An electrical resistance furnace under a protective atmosphere of Ar and SF_6 was used to melt the alloys. Initially, solid Mg was molten by heating it up to 700 °C. When molten, the pre-heated Si granulates at 400 °C were added and the mixture was stirred with a steel paddle every 5 minutes to improve the homogeneity. The mixture was maintained at 700°C during 20 minutes in order to favour the solubility of Si. Then preheated Sr chips at 400°C were added after which an exothermic reaction occurred. The furnace is then switched off and the temperature of the melt increased to the range of 750-850°C. The mixture was stirred and oxide products formed on top of the melt were removed. When the temperature of the melt was cooled down to 700°C the molten alloy was poured into a preheated steel die held at 400 °C during 45 minutes. Hexagonal BN was used as a mould release agent. After two minutes, the die was opened and the alloys were cooled down to room temperature (RT) by air cooling.

Disk shaped specimens were cut for microstructural characterization with 2 mm height and 18 mm diameter from the centre of the 20 cm long cast specimens. These disk samples were then ground and polished with water-free colloidal silica solution. Since burn-off takes place during preparation, the compositions after processing were measured by a Varian 720 ES inductively coupled plasma optical emission spectrometry (ICP-OES). The measurements are based on the comparison with standard curves previously calculated for the pure elements.

The microstructure was analysed using an optical microscope and a Philips XL30 FEI scanning electron microscope (SEM) equipped with an EDAX TSL energy dispersive X-ray spectroscopy (EDS) detector. Backscatter electron (BSE) images were used to identify the stoichiometry of the compounds. Due to the small size of the intermetallics an excess of Mg coming from the bulk is measured when identifying the compounds stoichiometry. The inflated Mg values are caused by the interaction volume reached during EDS analysis. This interaction volume is simulated in this work in order to compare it with the actual particle size. For this reason the ratio At%Si:At%Sr was considered as more reliable than the Mg percentage values. For the very small intermetallic particles (smaller than 1μm) field emission electron probe microanalyzer (EPMA), FEG EPMA JXA-5830F was used for detailed chemical analysis. The size of the intermetallic phases was measured by image analysis of the micrographs using Image-J software and the average values are presented in this paper.

X-ray diffraction (XRD) was done in a XRD Seifert 3003-TT device operating at 40kV and 40 mA and using Cu-Kα radiation. Scans were performed from 10 to 80 degrees with a 0.02 step size and measuring time of 2 seconds per step. The identification of the phases was done by comparison with the JCPDS cards included in the Pearson database. The used cards for Mg, M2, M17, M111 and M121 phases correspond to the numbers 00-035-0821, 00-035-0773, 03-065-3649, 01-089-1920 and 01-087-0897 respectively. The phase identification was performed both on the as-cast samples and after subsequent heat treatments. All X-ray diffraction tests were performed at room temperature.

The heat treatments done under argon inert atmosphere were followed by quenching in water at room temperature. A first heat treatment (HT1) was done during 48 hours at 500 °C and then a second one (HT2) during longer time (240 hours) and higher temperature (550 °C) was also applied to fully equilibrate the samples. Previous works involving Mg-rich intermetallic stability has been consulted to decide length of the HT to attain equilibrium. For instance Mg-Sn alloys have been described as fully homogenized after 96 hours at 320 °C [19], complete dissolution of Mg_2Si has been observed after 45 minutes at 525 °C [20] and good agreement with equilibrium calculations have been found for Mg-Ca-Zn alloys after a total 147 hours treatment at different temperatures [21]. The longest HT of 240 hours was found in the work of Nie and Muddle [22] were the thermal stability of compounds in Mg-Ca alloys was studied after heat treatments from 8 up to 240 hours.

4. Results

4.1. As cast condition

The compositions of the cast alloys (A to L) are given in table 3 together with the phase identification in the as-cast condition. From the experimental data (SEM-EDS, EPMA and XRD) four sets of co-existing phases have been found within the studied composition range: Mg+M17+M111, Mg+M17+M111+M121, Mg+M121 and Mg+M17+M121. The identification of the four different intermetallic phases based on SEM-EDS analysis is presented in figure 2. Values obtained from SEM-EDX and EPMA are summarized in table 4. The microstructure and the related XRD pattern of one representative sample from each set are discussed further. The rest of the samples in each set show similar structures as those presented. As an exception, samples C and F belonging to the same set are presented because they show different phases after equilibration.

Table 3. List of the studied alloys with their phase identification in the as-cast condition. Bold phases indicate the primary phase as expected from the calculated phase diagram.

Name	Composition at%		Phase identification	Si/Sr
	Si	Sr	As-cast	ratio
A	0.68	4.80	Mg+ M17+**M111**	0.14
B	0.63	3.09	Mg+ M17+M111+**M121**	0.20
C	1.20	3.75		0.32
D	1.41	2.65		0.53
E	2.50	1.62		1.54
F	0.33	0.14		2.36*
G	0.12	0.02	**Mg**+ M121	6.00*
H	0.41	0.07	Mg+M2+ **M121**	5.86*
I	5.31	0.96		5.53
J	4.60	0.82		5.61
K	3.40	0.75		4.53
L	3.17	0.90		3.52

* In alloys F, G and H the concentration of Sr is below the reliable detection limit. The amount of Sr is expected to be higher than the measured value. The presented values are based on extrapolated points from the standard ICP curves since interpolation was not possible for amounts smaller than 0.5 at% Sr.

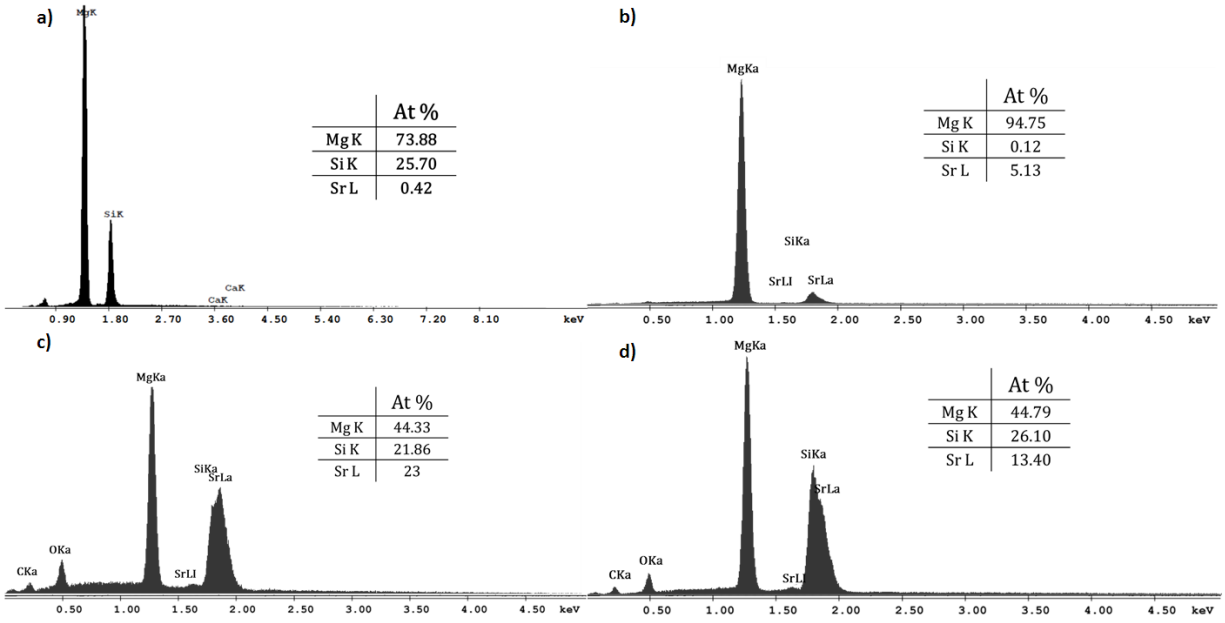

Figure 2. Identification of the intermetallic phases by SEM-EDS a)Mg_2Si b)$Mg_{17}Sr_2$ c)MgSiSr and d) $MgSi_2Sr$.

Table 4. Identification of the intermetallic phases based on element quantification by SEM-EDS analysis.

Alloy	Phase	Condition	Elements (At%)			Ratio (At%) Si:Sr
			Mg	Si	Sr	
A	M111	As Cast	54.7	21.13	23.02	0.92
		HT1	40.92	33.13	25.83	1.28
		HT2	46.68	26.07	25.23	1.03
	M17	As Cast	94.13	0.01	5.87	
		HT1	91.32	0.7	7.98	
		HT2	90.05	0.56	9.39	
C	M111	As Cast	51.56	23.17	25.27	0.92
		HT1	47.75	28.23	24.02	1.18
		HT2	36.65	32.6	27.63	1.18
	M121	As Cast	52.81	31.47	14.99	2.1
		HT1	55.5	27.95	16.61	1.68
	M17	As Cast	91.56	0.01	8.44	
		HT1	91.51	0.4	8.09	
		HT2	91.57	0.67	7.76	

Alloy	Phase	Condition	Elements (At%)			Ratio (At%) Si:Sr
			Mg	Si	Sr	
F	M111	As Cast	74.76	13.82	14.38	0.96
		HT1	46.85	29.95	23.23	1.29
		HT2	36.8*	32.59*	29.1*	1.12*
	M121	As Cast	59.68	26.54	13.77	1.93
		HT1	56.33	13.01	12.62	1.03
		HT2	68.9	21.46	9.64	2.23
	M17	As Cast	88.97	0.15	9.92	
G	M121	As Cast	87.38	8.24	4.38	1.88
		HT1	52.63*	34.5*	12.79*	2.70*
		HT2	93.38	4.71	1.9	2.48
K	M121	As Cast	57.68	30.25	12.07	2.51
		HT1	55.89	31.04	13.05	2.38
		HT2	53.79	32.42	13.79	2.35
	M2	As Cast	67.08	30.79	2.13	
		HT1	80.36	18.84	0.8	
		HT2	69.83	29.73	0.44	

* These values were obtained based on EPMA measurements.

The interaction volume used for EDS analysis has been simulated as a function of the energy applied and the selected elements. Based on these simulations the reliability of the phase composition was reduced in cases where the size of the intermetallic compounds was small. This happens for cases where the M111 and M121 particle size is smaller than 1 µm, which can be deduced from the calculations presented in Figure 3. In these cases the phase size may be much smaller than the interaction volume, making the results of the analysis coming partially from the bulk instead of from the selected particle. In these cases (M111 compound in alloy F and M121 in G), EPMA was used for detailed chemical analysis of the particles. The results are also presented in table 4.

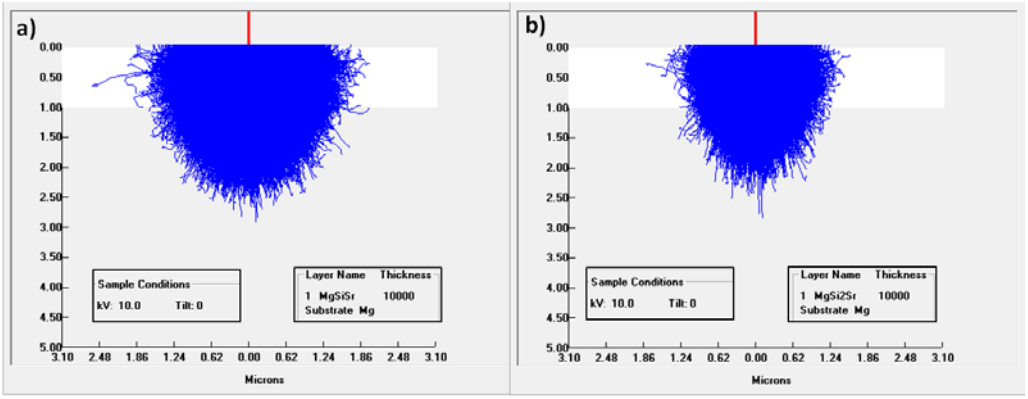

Figure 3. Interaction volume simulations of 1µm thickness particles of a)MgSiSr and b)$MgSi_2Sr$ in Mg matrix under 10 keV accelerating voltage.

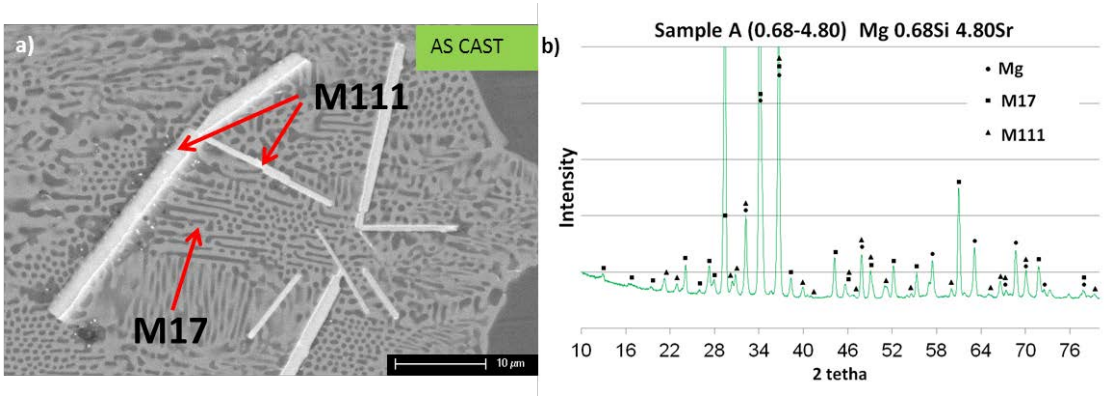

Figure 4. Identification of the intermetallic phases M17 and M111 in sample A (Mg 0.68Si 4.80Sr) a) BSE SEM micrograph and b) its XRD pattern.

Figure 4 shows alloy A. Both the micrograph (4a) and the XRD pattern (4b) clearly show the presence of the two intermetallic phases M17 and M111. The binary eutectic is dominating the microstructure in the as-cast condition. The residual dark grey phase corresponds to pure Mg. The ternary M111 appears in a needle like shape with a brighter white tone. Size and thickness of the M111 particles vary from 5 to 20 µm lengths and from 0.2 to 1 µm thickness. M111 appears surrounded by the eutectic, indicating that it was the primary forming phase.

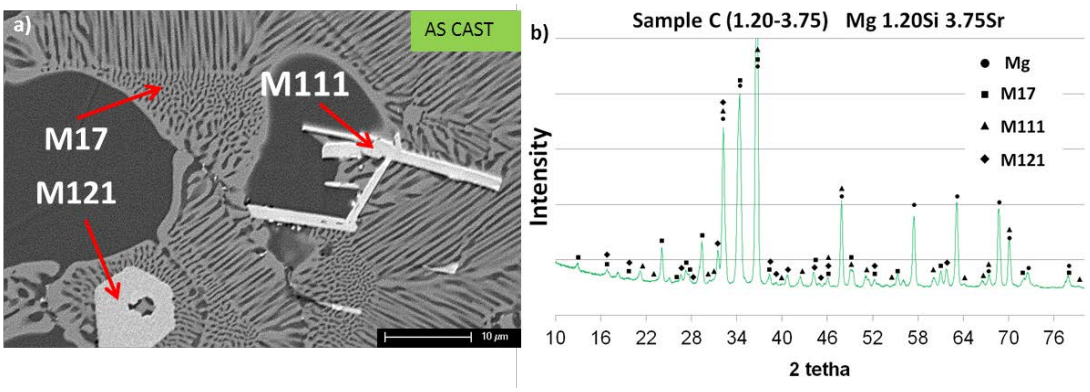

Figure 5. Identification of the secondary phases M17, M111 and M121 of the sample C (Mg 1.41Si 2.65Sr) in a) BSE SEM micrograph and b) its XRD pattern.

In alloy C, the ternary phases M111 and M121 and the binary phase M17 were identified from both the micrograph (figure 5a) and the XRD pattern (figure 5b). The binary eutectic is present in the whole surface with an aligned disposition and pure Mg is visible as dark islands in between. The ternary M111 appears similar as in alloy A (Figure 3a) in a white needle like shape. M121 presents a more angular greyish aspect. The size of the M111 particles ranges from 5 to 20 µm lengths with about 2 µm thickness. M121 presents a coarser polygonal shape with sizes from 10 to 50 µm and usually square holes in the central part. Also the M121 particles are enclosed by the eutectic indicating its earlier formation during solidification for this alloy.

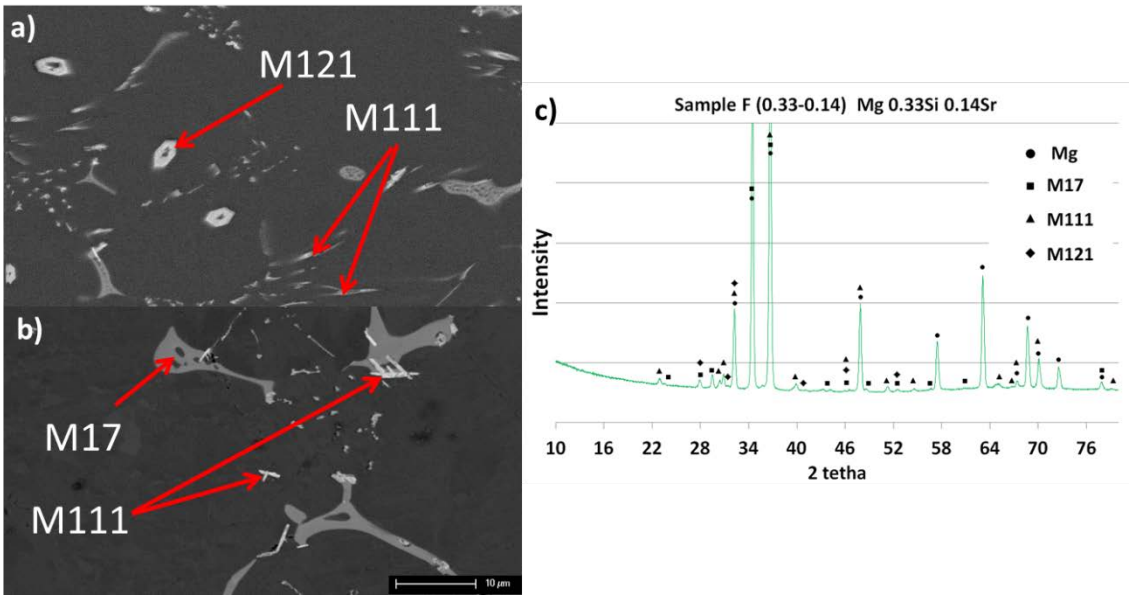

Figure 6. Identification of the intermetallic phases in sample F (Mg 0.33Si 0.14Sr) a) BSE SEM micrograph with M111 and M121, b) BSE SEM micrograph with M17 and M111 and c) all intermetallic phases identified in its XRD pattern.

For alloy F, the same phases are present as in alloy C but in a much lower amount and with a smaller size, as can be observed in the micrographs in figures 6a and 6b and in the peak intensities derived from the XRD pattern (figure 6c). In this case M121 is the primary phase as it took the Si and Sr from the liquid when growing, leaving regions rich in Mg behind which surround the polygonal ternary particles.

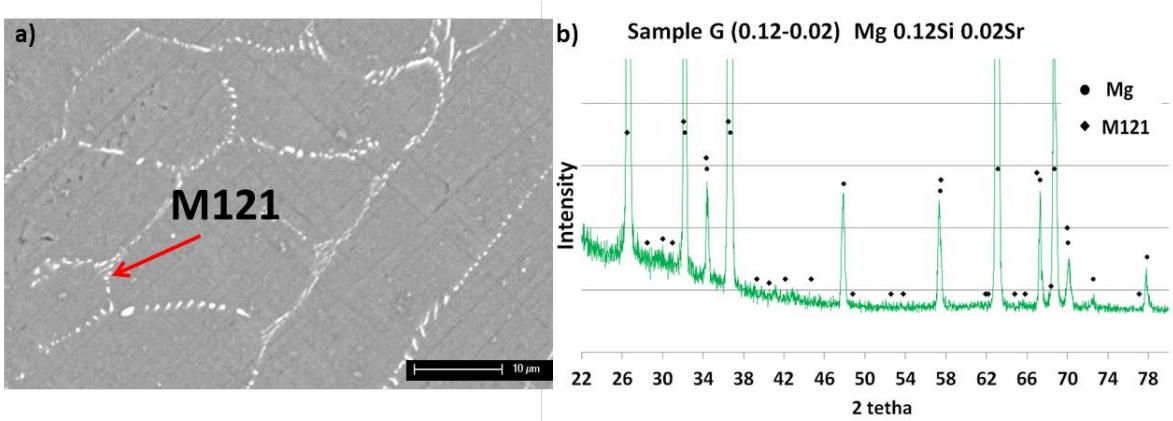

Figure 7. Identification of the ternary phase M121 in sample G (Mg 0.12Si 0.02Sr) from a) BSE SEM micrograph and b) its XRD pattern.

In alloy G the ternary M121 is identified. It is accumulated in between the Mg matrix (Figure 7a) and it is present in small dot like particles with a bright white colour. In this case, first Mg solidifies and then the intermetallic does; the ternary compound is then the secondary phase in this alloy. In this case the identification of the intermetallic phase in the XRD pattern (Figure 7b) is not evident since the amount of the M121 is minor compared with the pure Mg. The characteristic peaks are mixed with the Mg ones or vanished in the background.

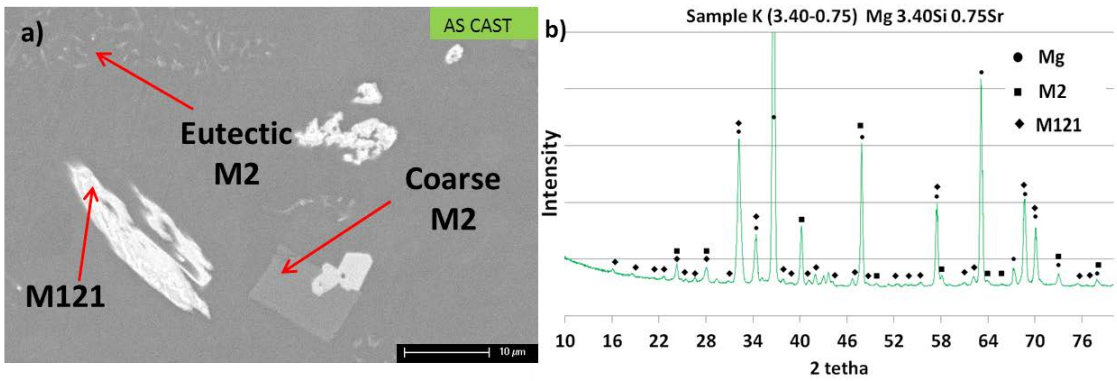

Figure 8. Identification of the secondary phases M2 and M121 in sample K (Mg 3.40Si 0.75Sr) in a) BSE SEM micrograph and b) its XRD pattern.

In sample K the binary phase formed is M2 having a light grey colour in the SEM micrograph shown in Figure 8a. Two typical morphologies of this phase that have been previously described, among others by Hu et al. [23], are observed. They are the coarse polygonal particles and the rod-like shaped eutectic ones. The latter is smaller in size and more homogeneously distributed in the sample surface. M121 also exists in this alloy appearing bright white due to the Sr content. The shape of this ternary varies from close to polygonal to irregular. Both intermetallics have been identified from the XRD pattern (Figure 8b).

4.2 After heat treatment

A first heat treatment (HT1) has been performed in an attempt to evaluate the near-equilibrium microstructure and phase composition. Then a second heat treatment (HT2) has been applied to the alloys. Even if it is difficult to go back from the as-cast condition to the equilibrium state, the alloys can be considered as equilibrated after HT2, as discussed in section 2. The results are summarized in table 5.

Table 5. List of the studied alloys with their phase identification in the equilibrated condition.

Name	Composition at%		Phase identification In equilibrium conditions	Si/Sr ratio
	Si	Sr		
A	0.68	4.80	Mg+ M17+M111	0.14
B	0.63	3.09		0.20
C	1.20	3.75		0.32
D	1.41	2.65		0.53
E	2.50	1.62	Mg+M111+M121	1.54
F	0.33	0.14		2.36*
G	0.12	0.02	Mg+ M121	6.00*
H	0.41	0.07	Mg+M2+ M121	5.86*
I	5.31	0.96		5.53
J	4.60	0.82		5.61
K	3.40	0.75		4.53
L	3.17	0.90		3.52

* In alloys F, G and H the concentration of Sr is below the reliable detection limit. The amount of Sr is expected to be higher than the measured value. The presented values are based on extrapolated points from the standard ICP curves since interpolation was not possible for amounts smaller than 0.5 at% Sr.

The identification of the phases according to the SEM-EDS analysis and to the XRD patterns for the alloys after HT1 and HT2 is discussed as follows and compared with the as-cast condition:

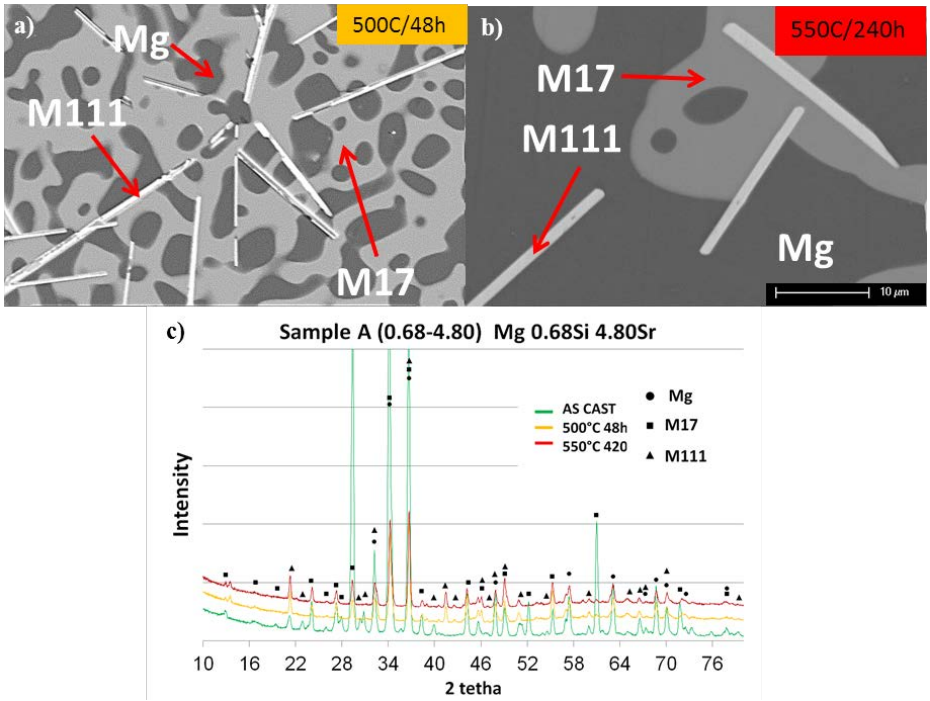

Figure 9. BSE SEM micrograph with labelled phases of the sample A a) after HT1 and b) after HT2. c) XRD pattern of sample A with the identified phases in as-cast condition and after the two HT.

In alloy A, the same phases M17 and M111 as in the as-cast condition are identified from the micrographs (figures 9a and 9b) and XRD peaks (figure 9c). The binary eutectic has been drastically reduced and presents a more globular form instead of the lamellar one present immediately after casting before the equilibration. The intensity of the M17 peaks is gradually reduced when increasing temperature and duration of HT, indicating a reduction in the amount of this phase from the as-cast to the equilibrium condition. The amount of pure Mg has increased and the amount of ternary M111 appears to be slightly reduced. The M111 particles are more homogeneous in size, with an average of 15 µm length and 1 µm thickness.

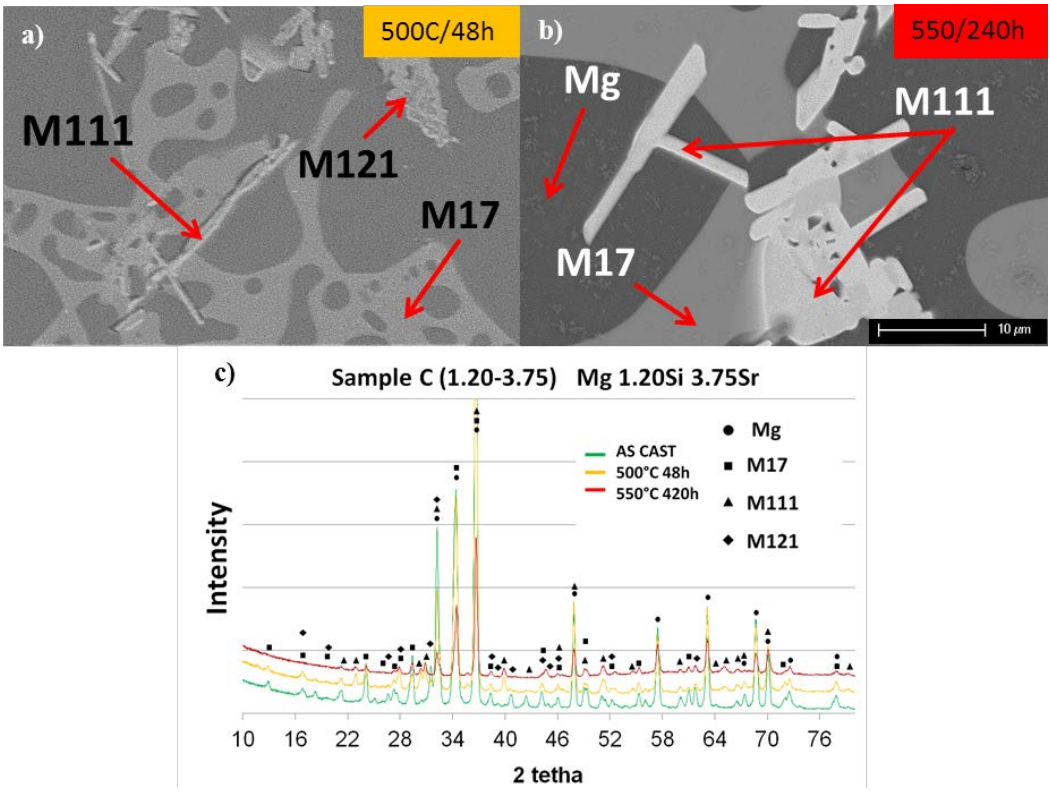

Figure 10. BSE SEM micrograph with labelled phases of the sample C a) after HT1 and b) after HT2. c) XRD pattern of sample C showing the phase identification in the as-cast condition and after the two HT.

In alloy C, three intermetallic phases together with the Mg are identified in the as-cast condition. When HT1 is applied, the M121 phase seems to lose the well-defined polygonal shape and starts dissolving (Figure 10a). Once equilibrium is reached, after HT2, the M121 does no longer exist (Figure 10b). The amount of binary M17 is reduced but still present after the HT2 and it is thus considered as an equilibrium phase. Similar for the M111 particles, their size (max 10 µm length) and number are reduced but they are still present in the equilibrium state.

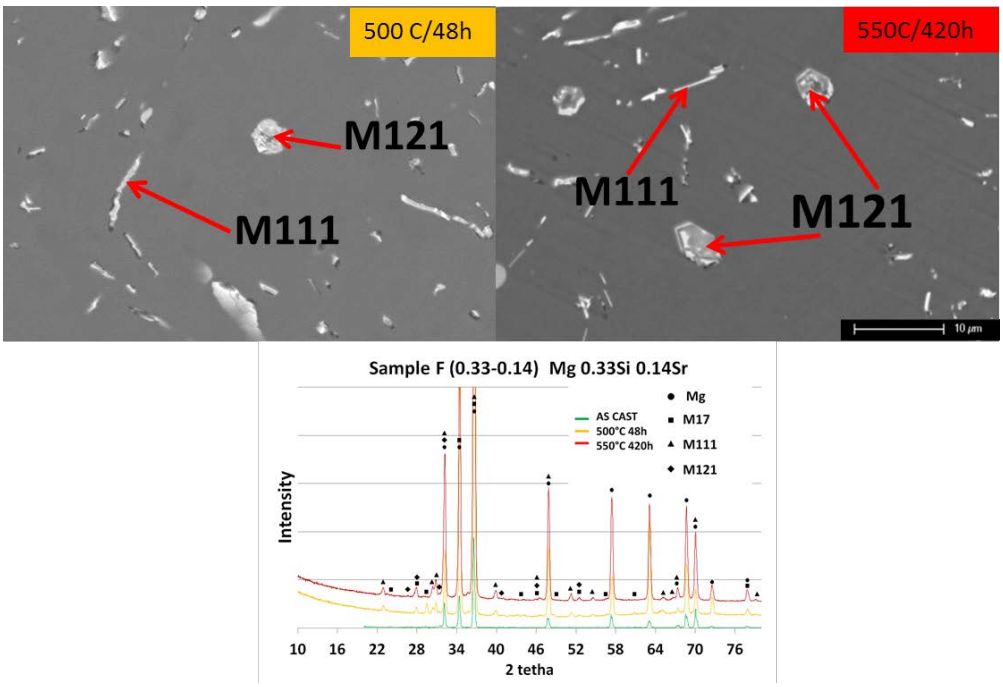

Figure 11. BSE SEM micrograph with labelled phases of the sample F a) after HT1 and b) after HT2. c) XRD pattern of sample F showing the phase identification in as-cast condition and after the two HT.

The alloy F presents a similar situation to the alloy C, where from the four phases observed in the as-cast condition (Figure 5) only three remain after HT1 and HT2. The binary M17 phase has dissolved and disappeared after the HT1 and HT2 (Figures 11a and 11b). The two ternary phases and pure Mg form the equilibrium phase combination (Figure 11c).

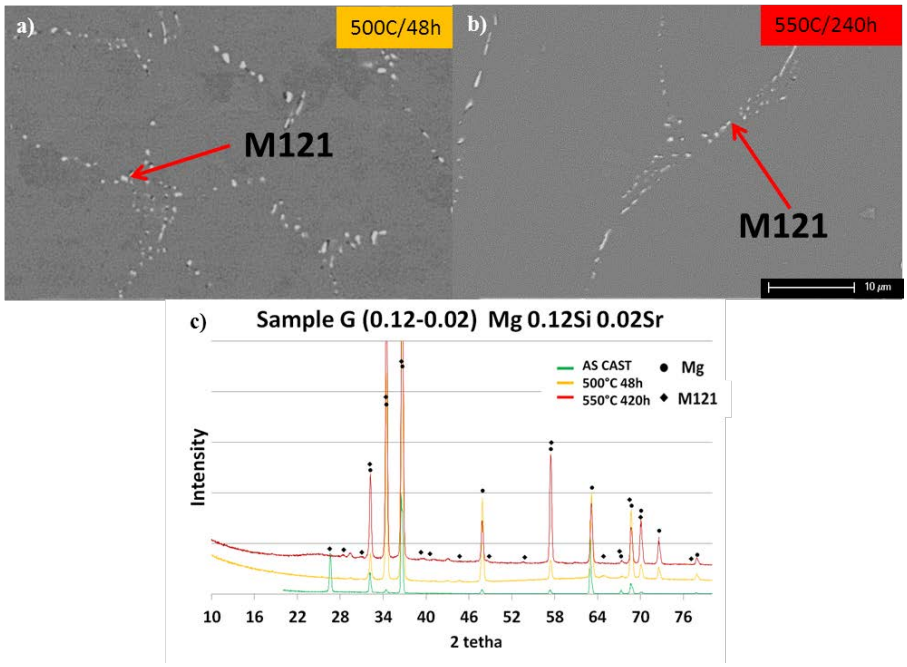

Figure 12. BSE SEM micrograph with labelled phases of the sample G a) after HT1 and b) after HT2. c) XRD pattern of sample G showing the phase identification in as-cast condition and after the two HT.

In alloy G the amount of ternary M121 phase is reduced with increasing time and temperature of the heat treatment as can be observed when comparing the figure 12a after HT1 and figure 12b after HT2 with figure 6a of the as-cast alloy. Its size and shape is similar as in the as-cast condition. From the XRD pattern the two intermetallics are still identified with the Mg matrix after equilibration (Figure 12c).

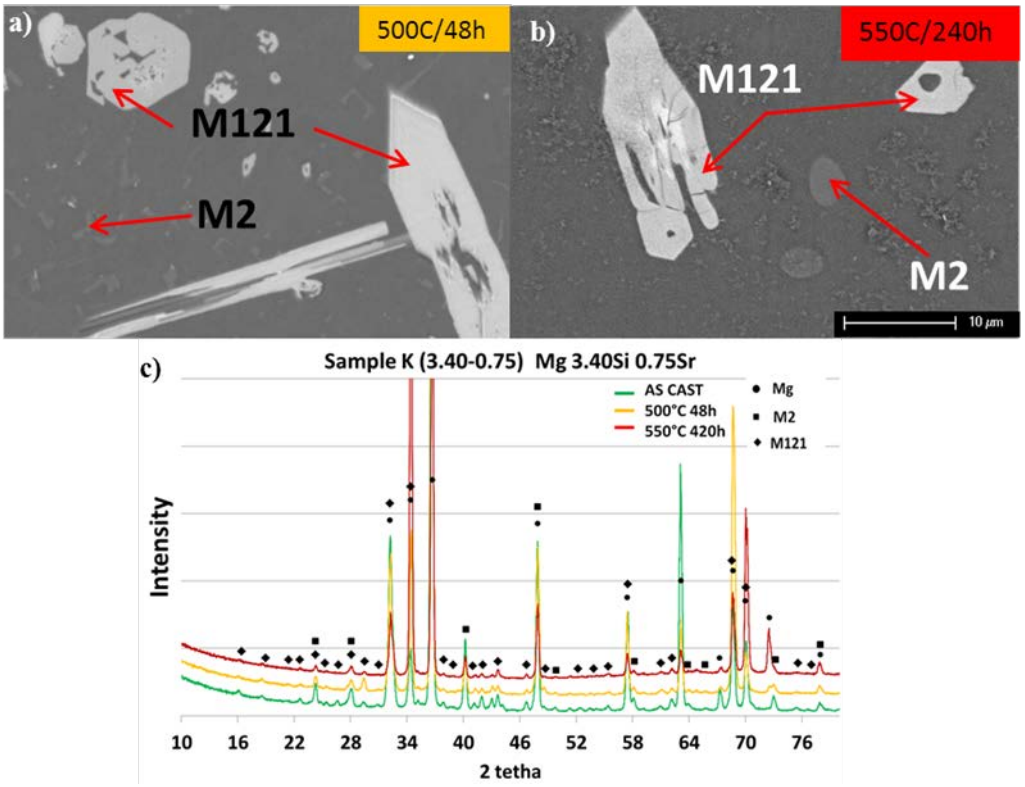

Figure 13. BSE SEM micrograph with labelled phases of the sample K a) after HT1 and b) after HT2. c) XRD pattern of sample K showing the phase identification in the as-cast condition and after the two HT.

In alloy K, the same phases are present before and after HT. The number and size of the M2 phase particles, in light grey in Figures 13a and 13b, reduced, but the phase remains present in the equilibrium microstructure. When analysing the XRD patterns (Figure 13c), the reduction in peak intensity is linked with the M2 phase, that has been partially dissolved after HT. The ternary M121 did not undergo significant modifications in size or shape from the as-cast condition compared to after the HT1 or HT2, but some gradation in colour is observed inside the particles (Figures 13a and 13b). A brighter region can be distinguished in the central part of the M121 particle while the external part is darker. The external darker area is richer in Si showing a difference in composition from the centre to the edges, solidification starts in the centre and excess of Si segregates towards the liquid enriching in Si the last solidifying part of the particles. At the same time some not well defined small particles are visible in alloy K after HT2 (Figure 13b), they are mainly Mg oxide generated at the surface during the heat treatment, possibly due to a reduction in the argon flux.

5. Discussion

When comparing Table 5 and Table 3, a difference in the phases present is observed between the equilibrium and as-cast alloys. This difference indicates that the as-cast alloys are not always in

equilibrium. This can be concluded as well from the coexistence of four phases observed in the as-cast alloys B to F. More than three different phases in a ternary system indicates a non-equilibrium structure as it violates Gibbs phase rule.

After the heat treatments a difference in microstructure has been observed for some of the studied alloys (B to F). The microstructures after heat treatment show that the M111 and M17 phases present in the as-cast condition were sometimes unstable, and therefore dissolve during equilibration. In the alloys B, C and D the disappearing phase was the ternary M111 while in E and F it was the binary M17. Finally, in all equilibrated alloys a maximum of 3 phases coexists together, in agreement with Gibbs phase rule applied to a system with 3 elements. For all samples, the phase combination present at equilibrium is presented in Table 5.

The sets of coexisting phases in equilibrium can be related with the experimental ratio At%Si:At%Sr and the results are presented in Table 5. We can distinguish four different regions, namely Mg+M17+M111 when the ratio At%Si:At%Sr is below 1, Mg+M111+M121 when the ratio is between 1 and 2.5, Mg+M2+M121 when the ratio is between 3 and 6 and Mg+M121 for the highest Si content.

The experimentally obtained phase regions after HT2 (from Table 5) can be compared with the predicted ones in the ternary diagram at 550 °C (Figure 14). This phase diagram was calculated using the thermodynamic description established as discussed in section 2 of this paper. Figure 14 shows a zoom of the Mg rich corner of the ternary diagram up to 6 at% in both Sr and Si at 550 °C. The relation established between the combination of coexisting equilibrium phases and the ratio At% Si:At % Sr obtained from the theoretical phase diagram calculation agrees well with the experimentally observed phases after heat treatment. It has to be taken into account that the At%Si:At%Sr ratio in alloys F, G and H were tenderly increased due to the low Sr amount detected in the ICP measurements. In cases where the Sr content was below 0.5 at%, the composition was calculated based on an extrapolated section of the standard curves, resulting in slightly smaller values than the real values. It can be read from the diagram that the region with Mg+M17+M111 is present when the ratio At%Si:At%Sr is below 1, the region with Mg+M111+M121 is present when the At%Si:At%Sr ratio is between 1 and 2, the one with Mg+M121 when the ratio is exactly 2 and the region with Mg+M2+M121 when the ratio is higher than 2. This good agreement between the theoretically predicted and the experimentally obtained phase regions indicates the soundness of our assumptions and the suggested phase diagram. However more thermodynamic data are needed for the complete description of the Mg-rich corner in the Mg-Si-Sr system.

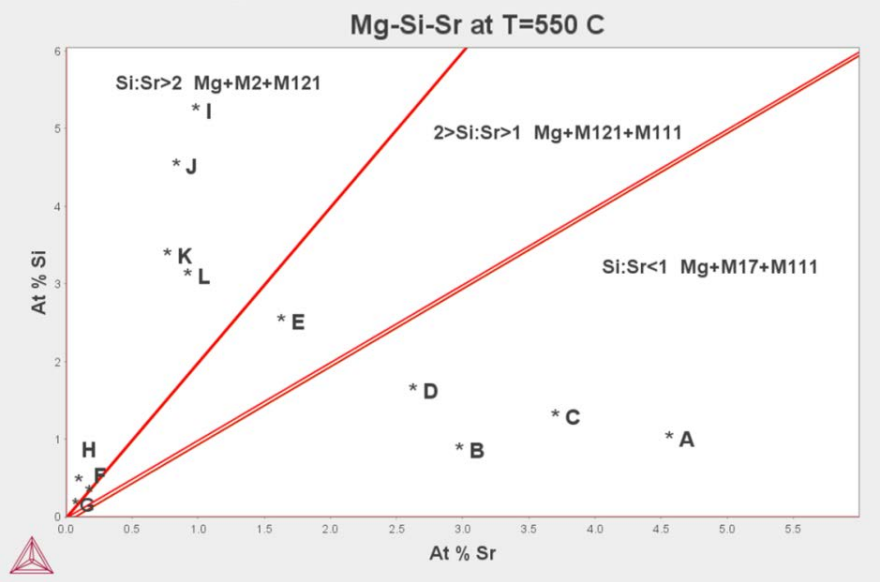

Figure 14. Distribution of the studied alloys (A-L) in the Mg rich corner at 550 °C of the ternary phase diagram within the different phase regions. The phase boundaries were calculated using the database developed in this work.

6. Conclusions

The presence of the two intermetallic ternary compounds MgSiSr and $MgSi_2Sr$ in the Mg-Si-Sr system has been identified by microstructure characterization. These two ternary compounds together with the binary compounds $Mg_{17}Sr_2$ and Mg_2Si make the four phases that cover the possible existing intermetallic combinations in the Mg rich corner of the Mg-Si-Sr alloy system.

The stability of the intermetallic phases has been shown at 500 °C and 550 °C after long heat treatments at these temperatures. On the one hand, the MgSiSr ternary compound is present in the as-cast specimens but in some cases it turned out to be a metastable phase since it disappears during annealing. In the rest of the cases, MgSiSr was an equilibrium phase and after some reduction in size and amount it remains stable during the heat treatment. The same happens with the binary $Mg_{17}Sr_2$ showing a tendency to disappear or decrease in amount compared to the as-cast condition. The binary eutectic shows a change from lamellar structure to a globular one. On the other hand, the ternary $MgSi_2Sr$ and the binary Mg_2Si are present in the as-cast condition and they both remain in the equilibrium microstructures. They do not present modifications with heat treatments, showing their stability at 500°C and 550 °C.

The expected combination of phases in equilibrium can be predetermined based on the At%Si:At%Sr ratio. A good agreement was found when comparing the experimental phases in the equilibrated alloys with the calculated isothermal section of the phase diagram at 550 °C. It can be concluded that the hypothesis that both ternary systems Mg-Ca-Si and Mg-Sn-Sr could be used as a guide for the thermodynamic description of the two ternary compounds in the Mg-Si-Sr system is realistic. Then, there may be a complete solubility between MgSiSr and Sr_2Si and the $MgSi_2Sr$ could be described as a stoichiometric compound.

Nevertheless, further work should be done in order to obtain a better thermodynamic description of the ternary system and a fully optimized Mg-Si-Sr database.

7. Acknowledges

The authors want to acknowledge for all the help and support during the processing of the alloys to Gabor Szakacs from Magic. The research was supported by the PEOPLE programme (Marie Sklodowska-Curie Action) of the EU FP7 Programme FP7/ 2007-2013/ under REA grant agreement n289163.

8. References

1. Witte, F., A. Eliezer, and S. Cohen. *The history, challenges and the future of biodegradable metal implants*. in *Advanced Materials Research*. 2010. Trans Tech Publ.
2. Kirkland, N., et al., *A survey of bio-corrosion rates of magnesium alloys.* Corrosion Science, 2010. **52**(2): p. 287-291.
3. Xin, Y., T. Hu, and P. Chu, *In vitro studies of biomedical magnesium alloys in a simulated physiological environment: a review.* Acta biomaterialia, 2011. **7**(4): p. 1452-1459.
4. Xin, Y., T. Hu, and P.K. Chu, *Degradation behaviour of pure magnesium in simulated body fluids with different concentrations of HCO 3.* Corrosion Science, 2011. **53**(4): p. 1522-1528.
5. Chen, S.L., et al., *The PANDAT software package and its applications.* Calphad, 2002. **26**(2): p. 175-188.
6. Andersson, J.O., et al., *Thermo-Calc & DICTRA, computational tools for materials science.* Calphad, 2002. **26**(2): p. 273-312.
7. Bale, C.W., et al., *FactSage thermochemical software and databases.* Calphad, 2002. **26**(2): p. 189-228.
8. Bennett, J.W., et al., *Orthorhombic A B C Semiconductors as Antiferroelectrics.* Physical Review Letters, 2013. **110**(1): p. 017603.
9. B. Eisenmann, H.S., A. Weiss, *Z. Anorg. Allg. Chem.* . (1972). **391**: p. 241-264
10. Currao, A., Curda, J., Nesper, R., Z. Anorg. Allg. Chem., 1996. **622** p. 85-94.
11. Nesper, R., Currao, A., Angew. Chem., Int. Ed., 37, 1998. **841**.
12. Nesper, R., Wengert, S., Zuercher, F., Currao, A., Chem. Eur. J., 1999. **5**: p. 3382.
13. Gröbner, J., I. Chumak, and R. Schmid-Fetzer, *Experimental study of ternary Ca–Mg–Si phase equilibria and thermodynamic assessment of Ca–Si and Ca–Mg–Si systems.* Intermetallics, 2003. **11**(10): p. 1065-1074.
14. Zhou, B.-C., S.-L. Shang, and Z.-K. Liu, *First-principles calculations and thermodynamic modeling of the Sn−Sr and Mg−Sn−Sr systems.* Calphad, 2014. **46**: p. 237-248.
15. Schick, M., et al., *Combined ab initio, experimental, and CALPHAD approach for an improved thermodynamic evaluation of the Mg–Si system.* Calphad, 2012. **37**: p. 77-86.
16. Zhong, Y., et al., *Thermodynamics modeling of the Mg–Sr and Ca–Mg–Sr systems.* Journal of Alloys and Compounds, 2006. **421**(1–2): p. 172-178.
17. Garay, A., et al., *Thermodynamic modeling of the Si–Sr system.* Calphad, 2009. **33**(3): p. 550-556.
18. Dinsdale, A.T., *SGTE data for pure elements.* Calphad, 1991. **15**(4): p. 317-425.
19. Avraham, S., A. Katsman, and M. Bamberger, *Optimization of composition and heat treatment design of Mg–Sn–Zn alloys via the CALPHAD method.* Journal of Materials Science, 2011. **46**(21): p. 6941-6951.
20. Chaudhury, S. and D. Apelian, *Fluidized bed heat treatment of cast Al-Si-Cu-Mg alloys.* Metallurgical and Materials Transactions A, 2006. **37**(7): p. 2295-2311.
21. Levi, G., et al., *Solidification, solution treatment and age hardening of a Mg–1.6 wt.% Ca–3.2 wt.% Zn alloy.* Acta Materialia, 2006. **54**(2): p. 523-530.
22. Nie, J.F. and B.C. Muddle, *Precipitation hardening of Mg-Ca(-Zn) alloys.* Scripta Materialia, 1997. **37**(10): p. 1475-1481.
23. Hu, J.-l., et al., *Modification of Mg 2 Si in Mg-Si alloys with neodymium.* Transactions of Nonferrous Metals Society of China, 2013. **23**(11): p. 3161-3166.